Images of surface volatiles in Mercury's polar craters acquired by the MESSENGER spacecraft

Nancy L. Chabot[1]*, Carolyn M. Ernst[1], Brett W. Denevi[1], Hari Nair[1], Ariel N. Deutsch[1], David T. Blewett[1], Scott L. Murchie[1], Gregory A. Neumann[2], Erwan Mazarico[2], David A. Paige[3], John K. Harmon[4], James W. Head[5], and Sean C. Solomon[6,7]

[1]The Johns Hopkins University Applied Physics Laboratory, Laurel, Maryland 20723, USA
[2] Goddard Space Flight Center, National Aeronautics and Space Administration, Greenbelt, Maryland 20771, USA
[3]Department of Earth, Planetary, and Space Sciences, University of California, Los Angeles, California 90095, USA
[4]National Astronomy and Ionosphere Center, Arecibo Observatory, Arecibo, Puerto Rico 00612, USA
[5]Department of Geological Sciences, Brown University, Providence, Rhode Island 02912, USA
[6]Lamont-Doherty Earth Observatory, Columbia University, Palisades, New York 10964, USA
[7]Department of Terrestrial Magnetism, Carnegie Institution of Washington, Washington, D.C. 20015, USA

ABSTRACT

Images acquired by NASA's MESSENGER spacecraft have revealed the morphology of frozen volatiles in Mercury's permanently shadowed polar craters and provide insight into the mode of emplacement and evolution of the polar deposits. The images show extensive, spatially continuous regions with distinctive reflectance properties. A site within Prokofiev crater identified as containing widespread surface water ice exhibits a cratered texture that resembles the neighboring sunlit surface except for its uniformly higher reflectance, indicating that the surficial ice was emplaced after formation of the underlying craters. In areas where water ice is inferred to be present but covered by a thin layer of dark, organic-rich volatile material, regions with uniformly lower reflectance extend to the edges of the shadowed areas and terminate with sharp boundaries. The sharp boundaries indicate that the volatile deposits at Mercury's poles are geologically young, relative to the time scale for lateral mixing by impacts, and either are restored at the surface through an ongoing process or were delivered to the planet recently.

INTRODUCTION

More than two decades ago, Earth-based radar observations revealed that portions of Mercury's polar regions have high radar backscatter and circular polarization ratios, characteristics interpreted to be indicative of water ice deposits located within areas of permanent shadow (Slade et al., 1992; Harmon and Slade, 1992; Butler et al., 1993; Harmon et al., 2011). Since insertion into orbit about Mercury in 2011, the MErcury Surface, Space ENvironment, GEochemistry, and Ranging (MESSENGER) spacecraft has acquired abundant additional evidence that Mercury's polar regions host water ice and other frozen volatiles. MESSENGER images confirm that these deposits receive no direct sunlight (Chabot et al., 2012, 2013); active measurements of surface reflectance at 1064 nm reveal areas of anomalously high and low reflectance (Neumann et al., 2013); thermal models indicate that surface temperatures are consistent with the long-term retention of water ice (Paige et al., 2013); and neutron spectrometry indicates hydrogen-rich material within the polar deposits (Lawrence et al., 2013).

Not heretofore known, however, is the morphology of these deposits. In this paper we report on the first images from MESSENGER's campaign to resolve Mercury's permanently shadowed polar deposits and assess therefrom their mode of emplacement and evolution. Despite the fact that polar deposits are in permanent shadow, the MESSENGER imaging system is sufficiently sensitive to obtain images of the deposit surfaces with the very low levels of light scattered from illuminated crater walls. MESSENGER's Mercury Dual Imaging System (MDIS) (Hawkins et al., 2007) has a wide-angle camera (WAC) equipped with a broadband clear filter (700 nm central wavelength, 600 nm bandwidth) that can image the floors of north polar craters at a pixel scale of ~100 m.

IMAGES OF FROZEN VOLATILES ON MERCURY

The permanently shadowed interior of Prokofiev (112 km in diameter) exhibits evidence for surficial water ice, on the basis of high reflectance values measured by MESSENGER's Mercury Laser Altimeter (MLA) (Neumann et al., 2013) and thermal model predictions for water ice stability (Paige et al., 2013). The WAC broadband images in Figure 1 provide the first views at visible wavelengths of the radar-bright, shadowed surface within Prokofiev and reveal a portion of the crater floor that has a higher reflectance than its surroundings. The high-reflectance surface has been identified in two WAC broadband images acquired under different illumination conditions (Figs. 1C and 1D), indicating that the higher reflectance is indicative of the properties of the surface rather than an artifact of a particular scattered lighting geometry. Scattered-flux illumination calculations (Mazarico et al., 2011) performed with an MLA-derived digital elevation model also support the inference that the high reflectance of this surface is not caused by viewing geometry.

The surface texture of the radar-bright region in Prokofiev does not differ from that of the portion of the crater floor that receives periods of direct solar illumination when viewed at this scale (85 m/pixel). The images reveal that the higher-reflectance region is fairly uniform, not patchy as would be expected if surface ice had predated the small craters and associated ejecta had buried portions of it. Estimates of the thickness of water ice deposits range from a minimum of several meters (Harmon, 2007) to an upper limit of a few hundred meters (Talpe et al., 2012). If the brighter region is water ice exposed on the surface, its thickness also does not noticeably affect the texture of the surface at this scale. As measured for the illumination conditions in the images, the higher-reflectance region has 4%–5% greater relative reflectance than the immediately neighboring non-radar-bright surface. Given the complex illumination conditions, determination of absolute reflectance values would require more detailed modeling of the multiply scattered sunlight incident on each surface. The MLA reflectance at 1064 nm measured within Prokofiev is about a factor of two higher than the surrounding terrain (Neumann et al., 2013); the larger reflectance difference is consistent with the low phase angle of the MLA observations in comparison with that of the images and the fact that ice shows a larger relative increase in reflectance at low phase angles than most other materials (Verbiescer et al., 2013).

Thermal models predict that the four large craters hosting radar-bright material north of Prokofiev are also capable of sustaining water ice at the surface (Paige et al., 2013), and MLA measurements interior to one of those craters, Kandinsky, suggest higher reflectance values (Neumann et al., 2013). The floors of these four craters (Fig. 2) show surface textures marked by small craters that do not look atypical for crater floors on Mercury. Unlike Prokofiev, the entire floors of these high-latitude craters are in

*E-mail: Nancy.Chabot@jhuapl.edu.

GEOLOGY, December 2014; v. 42; no. 12; p. 1051–1054; Data Repository item 2014363 | doi:10.1130/G35916.1 | Published online 15 October 2014

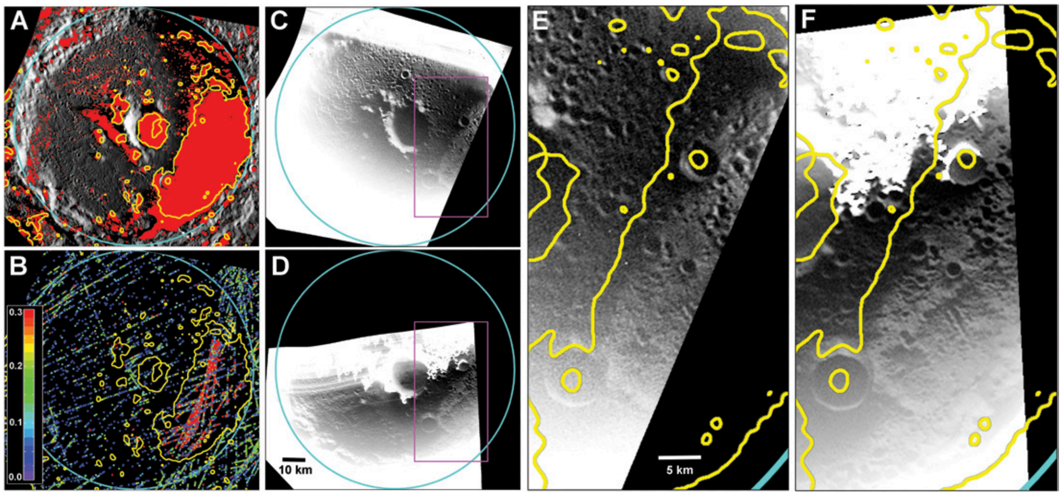

Figure 1. High-reflectance surface within Prokofiev crater, Mercury. The rim of the 112-km-diameter Prokofiev crater is outlined in cyan. All images are in stereographic projection about the north pole, with 180°E to the top. A: The radar-bright region (yellow outline; Harmon et al., 2011) is located within the persistently shadowed region (red) determined from every available Mercury Dual Imaging System image. B: Mercury Laser Altimeter reflectance values (color bar) at 1064 nm (Neumann et al., 2013) are higher in the radar-bright region. C: A wide-angle camera (WAC) broadband image reveals an area of higher reflectance on the crater floor (pink box). D: A second WAC broadband image acquired under different illumination shows the same higher-reflectance surface. E: Expanded view of the area within the pink box in C. F: Expanded view of the area within the pink box in D.

permanent shadow, so clear reflectance boundaries are not expected. The WAC broadband images reveal that the floor of Kandinsky (Fig. 2D) is less cratered than the other three, suggesting that Kandinsky is the youngest. Secondary cratering from Kandinsky may be responsible for many of the small craters on the floors of the other three large craters as well as Prokofiev. If so, the emplacement of surface water ice in Prokofiev must postdate the formation of Kandinsky.

In contrast to Prokofiev, for all other north polar craters equatorward of 86°N that host regions of permanent shadow and for which WAC broadband filter images have successfully been acquired, the shadowed region has an anomalously low-reflectance surface. Scattered-flux illumination calculations (Mazarico et al., 2011) performed with an MLA-derived digital elevation model do not show any evidence that the low reflectance of the surface is the result of the scattered illumination geometry or doubly shadowed conditions. In these locations, MLA measurements also indicate low reflectance values (Neumann et al., 2013), and thermal models predict that

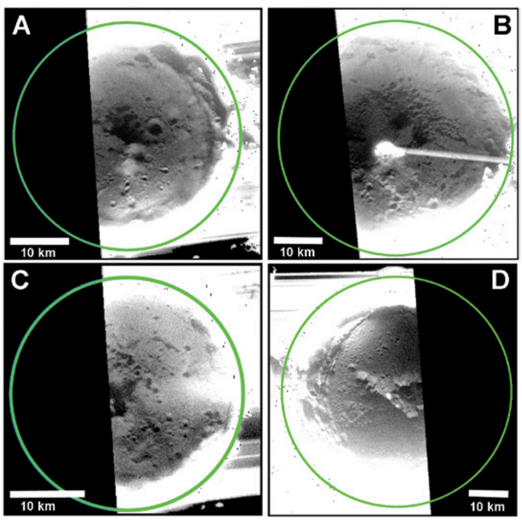

Figure 2. Surfaces within Mercury's permanently shadowed craters at the highest northern latitudes. Broadband wide-angle camera images (crater rims in green). All images are in stereographic projection about the north pole, with 180°E to the top. A: Chesterton (37 km diameter). B: Tolkien (50 km diameter); the streak is from the sunlit central peak. C: Tryggvadottir (31 km diameter). D: Kandinsky (60 km diameter).

any long-lived water ice must be buried beneath an insulating layer a few tens of centimeters in thickness (Paige et al., 2013). The observation of a higher-reflectance region in Prokofiev but lower-reflectance surfaces within permanently shadowed craters with warmer average surface temperatures supports the interpretation that the insulating layer is a lag deposit composed of low-albedo, cold-trapped, organic-rich, volatile material stable at temperatures somewhat higher than water ice. From WAC broadband images, the low-reflectance material is ~5%–25% lower in relative reflectance at these illumination conditions than the nearby crater floor, compared with a factor of ~2 difference detected by MLA (Neumann et al., 2013), consistent with the large difference in phase angle and the fact that low-reflectance materials such as carbon have relatively small increases in reflectance at low phase angles compared with other materials (Belskaya et al., 2008).

For the craters in Figure 3 that host large radar-bright regions (Figs. 3C–3E), the radar-bright deposit is collocated with the low-reflectance surface seen in the MDIS images. Three of the six examples in Figure 3 do not exhibit large regions of high radar backscatter in the Earth-based observations (Harmon et al., 2011) (Figs. 3B, 3F, and 3G). These regions had less favorable viewing geometries during ground-based radar observations, however, so polar deposits in these craters may not have been detected because of observational limitations. Nonetheless, an absence of ice in these areas cannot be excluded.

In the WAC broadband images, the low reflectance of the deposits appears uniform rather than patchy at the ~100 m pixel scale of the images. Small craters (~0.5–1 km in diameter) are visible within the low-reflectance surfaces seen in Figures 3F and 3G. These small craters do not have brighter ejecta associated with them, despite having excavated to depths substantially greater than the tens of centimeters thickness estimated for the low-reflectance deposits (Paige et al., 2013; Lawrence et al., 2013). In the WAC broadband images, the low-reflectance deposits have sharp boundaries that match closely with the boundaries of both the areas of persistent shadow and radar-bright regions, an example of which is shown for Berlioz crater in Figure 4. None of these boundary types are confined to topographic lows. Low-reflectance material extends up the crater walls to just below the rim in the examples in Figures 3 and 4, notwithstanding that elsewhere on Mercury relatively bright material can be exposed on crater walls by slumping. A table listing the locations and WAC image files for each crater shown in Figures 1–4 is provided in the GSA Data Repository[1].

[1]GSA Data Repository item 2014363, Table DR1 (locations and wide-angle camera image files for each crater), is available online at www.geosociety.org/pubs/ft2014.htm, or on request from editing@geosociety.org or Documents Secretary, GSA, P.O. Box 9140, Boulder, CO 80301, USA.

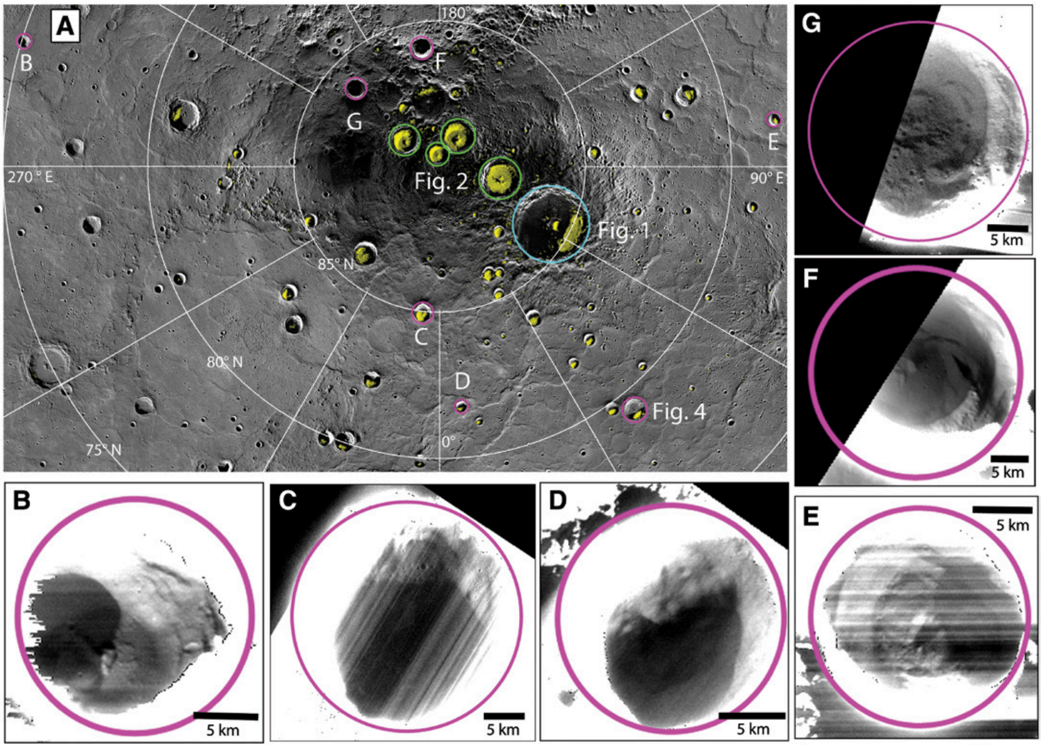

Figure 3. A: Mercury Dual Imaging System mosaic of Mercury's north polar region, highlighting craters from Figures 1 and 2 and craters for which broadband wide-angle camera images reveal low-reflectance deposits (rims in pink; see Fig. 4). All images are in stereographic projection about the north pole, with 180°E to the top. (A) Areas of high radar backscatter (Harmon et al., 2011) are shown in yellow. B: 17-km-diameter crater. C: Remarque (26 km diameter). D: 16-km-diameter crater. E: 17-km-diameter crater. F: 27-km-diameter crater. G: 28-km-diameter crater.

DISCUSSION AND IMPLICATIONS

In Prokofiev, the boundaries of the shadowed and radar-bright regions match closely (Fig. 1A), but the boundary of the high-reflectance region is offset inward by ~3 km relative to these other two boundaries. The intervening ~3-km-wide region has a relative reflectance that is not distinguishable from the neighboring surface that receives solar illumination. Studies of mare-highland contacts on the Moon indicate that impact gardening has achieved lateral transport over a scale of ~4–5 km (Li and Mustard, 2000), a scale comparable to the difference in boundary position between the high-reflectance region and the area of shadow in Prokofiev. If lateral mixing has covered the outermost edge of the surface ice deposit in Prokofiev, then the timing or rate of emplacement of water ice here was not so recent or so rapid, respectively, as to obscure the effects of lateral transport. Lateral mixing at lunar mare-highland contacts has operated over billions of years, though the minimum amount of time needed to form the lateral mixing zone is not known. The higher frequency and generally higher velocity of impacts at Mercury relative to the Moon (Cintala, 1992) could have led to more efficient lateral transport over shorter time scales.

Alternatively, although high-fidelity thermal models of the Prokofiev region at a resolution comparable to the WAC broadband images are not yet available, thermal models generally predict that areas of surface ice tend to be surrounded by a marginal zone of subsurface ice (Paige et al., 2010, 2013). The WAC images, in contrast, do not show evidence for a marginal zone of low-reflectance material in Prokofiev similar to the low-reflectance deposits associated with subsurface ice observed in other craters farther from the pole. Thus if the lesser dimensions of the high-reflectance region in Prokofiev are because only subsurface water ice is stable beneath a marginal zone, then the thermal environment in that zone must be different from that of the craters that host low-reflectance material. Early thermal models predicted that subsurface ice does not exist in

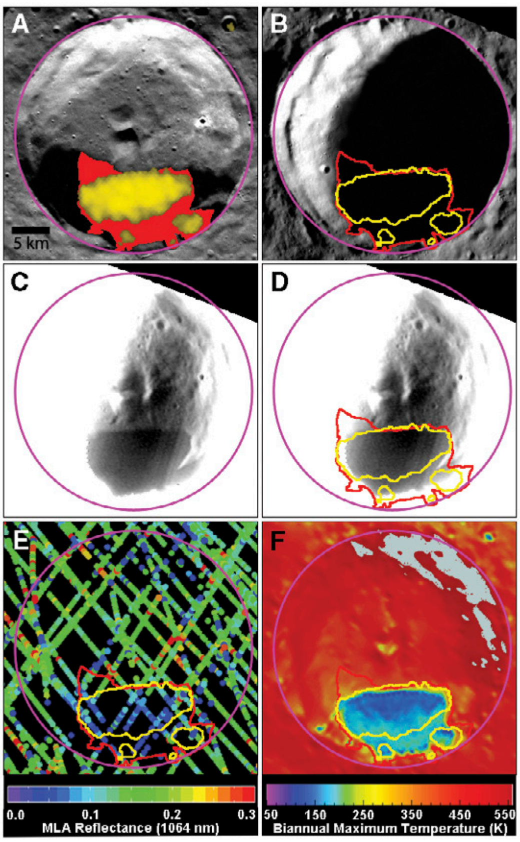

Figure 4. Low-reflectance material in 31-km-diameter Berlioz crater; the rim of the crater is outlined in pink. All images are in stereographic projection about the north pole; north is to the top. A: Radar-bright (yellow; Harmon et al., 2011) and persistently shadowed (red) regions are collocated. B: Illumination conditions ~20 h prior to acquiring the image in C. C: Wide-angle camera broadband image reveals low-reflectance material. D: Low-reflectance area extends to the edge of the radar-bright and persistently shadowed regions. E: Reflectance values measured by the Mercury Laser Altimeter (MLA; Neumann et al., 2013). F: Calculated maximum surface temperatures (Paige et al., 2013).

areas that are periodically sunlit (Vasavada et al., 1999), but perhaps the specific topography and location of Prokofiev create a thermal regime that can maintain subsurface ice even though the surface periodically reaches temperatures too high for the preservation of the low-reflectance organic-rich volatile material.

In the lower-latitude craters, the fact that the low-reflectance deposits display sharp boundaries that extend to the edges of the shadowed and radar-bright regions (Fig. 4) contrasts with the 3 km offset of such boundaries observed in Prokofiev and indicates that lateral mixing has not moved the boundary of low-reflectance material inward. This observation implies that the low-reflectance deposits formed geologically recently or as part of an ongoing process. However, if impact gardening of a low-reflectance deposit tens of centimeters thick exposed or thermally disturbed underlying water ice, any water ice exposed at the surface would quickly sublimate (1 m in 10^6 yr at 130 K; 1 m in 10^3 yr at 150 K; Vasavada et al., 1999; Paige et al., 2013). A stable configuration would rapidly be restored, perhaps resulting in the formation of new lag deposits of low-reflectance material. Thus, by continually disturbing and reforming the edges of the low-reflectance deposits, the impact gardening process potentially could keep the boundaries sharp and well matched to those of the radar-bright and permanently shadowed regions.

The total amount of ice at Mercury's poles is substantial, with estimates of ~10^{16}–10^{18} g (Moses et al., 1999; Lawrence et al., 2013). The upper estimate is comparable to the water volume of Lake Ontario (North America; ~1.64×10^{18} g) and consistent with delivery by external sources to Mercury and subsequent thermal stability over billions of years (Moses et al., 1999; Paige et al., 2013). However, in addition to lateral mixing, other processes have been suggested that would disrupt exposed volatile deposits on Mercury within geologically short time scales. Models of vertical mixing by impact gardening (Crider and Killen, 2005) indicate that ice would be buried at a rate of 4×10^{-9} m/yr; destruction by Lyman alpha photodissociation may limit the lifetime of exposed ice (Morgan and Shemansky, 1991); and organic synthesis within ice bombarded by galactic cosmic rays, such as in Prokofiev, may darken the ice on time scales of tens of millions of years (Crites et al., 2013). Moreover, although laser reflectance measurements at 1064 nm have yielded higher reflectance values for permanently shadowed regions at the lunar poles, indicative of modest amounts of water frost or a reduction in the effectiveness of space weathering (Lucey et al., 2014), visible-wavelength imaging of permanently shadowed craters on the Moon (Haruyama et al., 2008; Speyerer and Robinson, 2013) has not revealed surfaces with anomalously high or low reflectance similar to those seen in WAC broadband images of Mercury. One explanation for differences between the Moon and Mercury could be that the volatile polar deposits on Mercury were recently emplaced. If Mercury's currently substantial polar volatile inventory is the product of the most recent portion of a longer process, then a considerable mass of volatiles may have been delivered to the inner Solar System throughout its history.

ACKNOWLEDGMENTS

The MESSENGER project is supported by the NASA Discovery Program under contracts NAS5-97271 to The Johns Hopkins University Applied Physics Laboratory and NASW-00002 to the Carnegie Institution of Washington. Blewett and Paige are supported by the MESSENGER Participating Scientist Program. We thank P.O. Hayne, P.G. Lucey, and C.D. Neish for insightful reviews and J.B. Murphy for editorial handling.

REFERENCES CITED

Belskaya, I.N., Levasseur-Regourd, A.-C., Shkuratov, Y.G., and Muinonen, K., 2008, Surface properties of Kuiper belt objects and centaurs from photometry and polarimetry, *in* Barucci, M.A., et al., eds., The Solar System beyond Neptune: Tucson, University of Arizona Press, p. 115–127.

Butler, B.J., Muhleman, D.O., and Slade, M.A., 1993, Mercury: Full-disk radar images and the detection and stability of ice at the north pole: Journal of Geophysical Research, v. 98, p. 15003–15023, doi:10.1029/93JE01581.

Chabot, N.L., Ernst, C.M., Denevi, B.W., Harmon, J.K., Murchie, S.L., Blewett, D.T., Solomon, S.C., and Zhong, E.D., 2012, Areas of permanent shadow in Mercury's south polar region ascertained by MESSENGER orbital imaging: Geophysical Research Letters, v. 39, L09204, doi:10.1029/2012GL051526.

Chabot, N.L., Ernst, C.M., Harmon, J.K., Murchie, S.L., Solomon, S.C., Blewett, D.T., and Denevi, B.W., 2013, Craters hosting radar-bright deposits in Mercury's north polar region: Areas of persistent shadow determined from MESSENGER images: Journal of Geophysical Research–Planets, v. 118, p. 26–36, doi:10.1029/2012JE004172.

Cintala, M.J., 1992, Impact-induced thermal effects in the lunar and mercurian regoliths: Journal of Geophysical Research, v. 97, p. 947–973, doi:10.1029/91JE02207.

Crider, D., and Killen, R.M., 2005, Burial rate of Mercury's polar volatile deposits: Geophysical Research Letters, v. 32, L12201, doi:10.1029/2005GL022689.

Crites, S.T., Lucey, P.G., and Lawrence, D.J., 2013, Proton flux and radiation dose from galactic cosmic rays in the lunar regolith and implications for organic synthesis at the poles of the Moon and Mercury: Icarus, v. 226, p. 1192–1200, doi:10.1016/j.icarus.2013.08.003.

Harmon, J.K., 2007, Radar imaging of Mercury: Space Science Reviews, v. 132, p. 307–349, doi:10.1007/s11214-007-9234-y.

Harmon, J.K., and Slade, M.A., 1992, Radar mapping of Mercury: Full-disk images and polar anomalies: Science, v. 258, p. 640–643, doi:10.1126/science.258.5082.640.

Harmon, J.K., Slade, M.A., and Rice, M.S., 2011, Radar imagery of Mercury's putative polar ice: 1999–2005 Arecibo results: Icarus, v. 211, p. 37–50, doi:10.1016/j.icarus.2010.08.007.

Haruyama, J., et al., 2008, Lack of exposed ice inside lunar south pole Shackleton crater: Science, v. 322, p. 938–939, doi:10.1126/science.1164020.

Hawkins, S.E., III, et al., 2007, The Mercury Dual Imaging System on the MESSENGER spacecraft: Space Science Reviews, v. 131, p. 247–338, doi:10.1007/s11214-007-9266-3.

Lawrence, D.J., et al., 2013, Evidence for water ice near Mercury's north pole from MESSENGER Neutron Spectrometer measurements: Science, v. 339, p. 292–296, doi:10.1126/science.1229953.

Li, L., and Mustard, J.F., 2000, Compositional gradients across mare-highland contacts: Importance and geological implication of lateral transport: Journal of Geophysical Research, v. 105, p. 20431–20450, doi:10.1029/1999JE001168.

Lucey, P.G., et al., 2014, The global albedo of the Moon at 1064 nm from LOLA: Journal of Geophysical Research–Planets, v. 119, p. 1665–1679, doi:10.1002/2013JE004592.

Mazarico, E., Neumann, G.A., Smith, D.E., Zuber, M.T., and Torrence, M.H., 2011, Illumination conditions of the lunar polar regions using LOLA topography: Icarus, v. 211, p. 1066–1081, doi:10.1016/j.icarus.2010.10.030.

Morgan, T.H., and Shemansky, D.E., 1991, Limits to the lunar atmosphere: Journal of Geophysical Research, v. 96, p. 1351–1367, doi:10.1029/90JA02127.

Moses, J.I., Rawlins, K., Zahnle, K., and Dones, L., 1999, External sources of water for Mercury's putative ice deposits: Icarus, v. 137, p. 197–221, doi:10.1006/icar.1998.6036.

Neumann, G.A., et al., 2013, Bright and dark polar deposits on Mercury: Evidence for surface volatiles: Science, v. 339, p. 296–300, doi:10.1126/science.1229764.

Paige, D.A., et al., 2010, Diviner lunar radiometer observations of cold traps in the Moon's south polar region: Science, v. 330, p. 479–482, doi:10.1126/science.1187726.

Paige, D.A., Siegler, M.A., Harmon, J.K., Neumann, G.A., Mazarico, E.M., Smith, D.E., Zuber, M.T., Harju, E., Delitsky, M.L., and Solomon, S.C., 2013, Thermal stability of volatiles in the north polar region of Mercury: Science, v. 339, p. 300–303, doi:10.1126/science.1231106.

Slade, M.A., Butler, B.J., and Muhleman, D.O., 1992, Mercury radar imaging: Evidence for polar ice: Science, v. 258, p. 635–640, doi:10.1126/science.258.5082.635.

Speyerer, E.J., and Robinson, M.S., 2013, Persistently illuminated regions at the lunar poles: Ideal sites for future exploration: Icarus, v. 222, p. 122–136, doi:10.1016/j.icarus.2012.10.010.

Talpe, M.J., Zuber, M.T., Yang, D., Neumann, G.A., Solomon, S.C., Mazarico, E., and Vilas, F., 2012, Characterization of the morphometry of impact craters hosting polar deposits in Mercury's north polar region: Journal of Geophysical Research, v. 117, E00L13, doi:10.1029/2012JE004155.

Vasavada, A.R., Paige, D.A., and Wood, S.E., 1999, Near-surface temperatures on Mercury and the Moon and the stability of polar ice deposits: Icarus, v. 141, p. 179–193, doi:10.1006/icar.1999.6175.

Verbiescer, A.J., Helfenstein, P., and Buratti, B.J., 2013, Photometric properties of solar system ices, *in* Gudipati, M.S., and Castillo-Rogez, J., eds., The Science of Solar System Ices: Astrophysics and Space Science Library, volume 356: New York, Springer, p. 47–72.

Manuscript received 23 May 2014
Revised manuscript received 29 August 2014
Manuscript accepted 31 August 2014

Printed in USA